

Ion and Water Dynamics in the Transition from Dry to Wet Conditions in Salt-doped PEG

Nico Marioni,[†] Oscar Nordness,^{‡,¶} Zidan Zhang,[†] Rahul Sujanani,^{‡,¶} Benny D.

Freeman,[†] Rachel A. Segalman,^{‡,¶} Raphaële J. Clément,^{*,‡} and Venkat Ganesan ^{*,†}

[†] McKetta Department of Chemical Engineering, The University of Texas at Austin, Austin,
Texas 78712, United States

[‡] Materials Department and Materials Research Laboratory, University of California Santa
Barbara, Santa Barbara, California 93106, United States

[¶] Department of Chemical Engineering, University of California Santa Barbara, Santa Barbara,
California 93106, United States

E-mail: rclement@ucsb.edu

E-mail: venkat@che.utexas.edu

Abstract

The influence of water content on ion and water transport mechanisms in polymer membranes under low to moderate hydration conditions remains poorly understood. In this study, we combine ion and water diffusivity (PFG-NMR) measurements with atomistic molecular dynamics simulations to better understand transport processes in hydrated salt-doped poly(ethylene glycol). Above the water percolation threshold, experimental and simulated diffusivities are in good agreement with free volume transport models. At low hydration levels, unlike dry systems, ion diffusion cannot be described by polymer segmental dynamics alone. We rationalize such observations by the interplay between ion-water and ion-polymer solvation of cations, and between ion-water and cation-anion

interactions for anions. Further, we demonstrate that a two-state model combining ion-water solvation and free volume transport can describe water dynamics across the entire hydration range of interest. Our findings provide a more encompassing analysis of ion and water transport in hydrated polyelectrolytes, specifically in the low hydration regime.

An understanding of the mechanisms underlying ion transport is central to the development of polymer electrolytes for energy storage,¹⁻⁵ water purification,⁶⁻⁸ and resource recovery^{9,10} applications. To this end, various models and correlations have been established to describe and predict ion diffusion and guide the rational design of polymers with improved performance. Ion diffusion in dry polymer electrolytes is well understood to be (inversely) related to the segmental dynamics of the polymer.¹¹⁻¹⁵ This correlation arises due to the important role played by ion-polymer solvation, such that ion diffusion is limited by the thermal fluctuations of the polymer chains, allowing for ion diffusion (hops) between solvation sites along a single chain or between chains.¹⁶ At the other extreme of hydration, ion and water transport in uncharged, highly swollen, percolated hydrogels have generally been described by hindered transport or free volume models through the aqueous domain, in which the influence of ion-polymer solvation is usually not considered a pertinent factor.¹⁷⁻¹⁹ For instance, the model of Mackie and Meares²⁰ assumes a swollen polymer matrix consists of a homogeneous, percolated water network, which serves as a continuous pathway for ion diffusion made tortuous by immobile polymer chains obstructing ion transport. The diffusivity, D_i , is then related to the water volume fraction, ϕ_w :

$$D_i = D_i^{\text{Soln}} \left(\frac{\phi_w}{2 - \phi_w} \right)^2 \quad (1)$$

where D_i^{Soln} is the diffusion coefficient of species i in bulk aqueous solution. An alternative model by Yasuda et al. based on the activated-state free volume theory of diffusion²¹, and the assumption

that the free volume intrinsic to the polymer and water are additive in a polymer-water mixture²², gives rise to the following relationship:

$$D_i = D_i^{\text{Soln}} \exp\left(-\frac{(1-\alpha)\beta\left(\frac{1-\phi_w}{\phi_w}\right)}{1+\alpha\left(\frac{1-\phi_w}{\phi_w}\right)}\right) \quad (2)$$

where α is a polymer-dependent parameter related to its free volume, and β is a penetrant-dependent parameter related to the size of the diffusing species (ions or water molecules).

While significant progress has been made in understanding ion transport mechanisms in the extremes of dry polymeric electrolytes and highly swollen polymer membranes, these fields have generally been developed independently, leading to knowledge gaps regarding transport in low to moderately hydrated polymer systems. Recently, significant interest has arisen in such a regime for energy storage applications.^{23–26} For example, aqueous solid polymer electrolytes (polymer and water-in-salt electrolytes) exhibit high ionic conductivities, preferential lithium transport, and improved safety compared to solid polymer electrolytes, as well as improved electrochemical stability compared to salt-in-water electrolytes.²⁷ The ability to control ion permeation and ionic conductivity in low to moderately hydrated polymer systems hinge on developing fundamental insights into the interplay between ion-ion, ion-polymer, and ion-water interactions, and the role of ion-polymer solvation, on ion transport in the transition between “dry” and “hydrated” polymer systems.

For brevity, the majority of the experimental methodology is presented in Section S1 of the Supporting Information. In short, samples were prepared using number average molecular weight $M_n = 2,000$ g/mol poly(ethylene glycol) dimethyl ether (PEG-DME) obtained from Millipore Sigma (CAS 24991-55-7), lithium bis(trifluoromethane)sulfonimide (LiTFSI) obtained from Solvionic (CAS 171611-11-3), and ultra-pure Milli-Q water. Samples were prepared

(Scheme S1) across 5 hydration levels, $\lambda = 0.063$ to 1 H₂O molecules per PEG oxygen atom (Table S2), at a constant salt loading of $[\text{PEG O}]/[\text{LiTFSI}] = 10$, where $[\text{PEG O}]$ and $[\text{LiTFSI}]$ are the moles of ether oxygens and salt in the sample, respectively. Pulse field gradient (PFG)-NMR measurements were performed on a 300 MHz (7.05 T) Bruker wide bore spectrometer equipped with a DiffBB broadband probe to measure ¹H (PEG-DME, water), ⁷Li (Li⁺), and ¹⁹F (TFSI⁻) self-diffusion coefficients. All measurements (See Figures S2 and S3) were performed at 343 K to ensure sufficiently fast (i.e., measurable) diffusion at low hydration conditions, while also preventing water evaporation at higher hydration levels.

Figure 1A displays the ion (Li⁺, TFSI⁻) and water diffusion coefficients, D_i (D_{PEG} are displayed in Figure S5), as a function of hydration, $\lambda = [\text{H}_2\text{O}]/[\text{PEG O}]$, where $[\text{H}_2\text{O}]$ is the moles of water in the sample, obtained from PFG-NMR. The ion diffusivities at dry conditions ($\lambda = 0$, hollow points) were obtained from similar experiments by Hayamizu et al.²⁸ (LiTFSI-doped PEG-DME, MW = 2,500 g/mol at 343 K, $[\text{PEG O}]/[\text{LiTFSI}] = 10$) and plotted for reference. As expected, both ion and water diffusivities increase with increasing hydration. Interestingly, we observe a significant diffusive speedup for Li⁺ relative to TFSI⁻ ions. Further, we observe a significant diffusive speedup of water molecules in the low hydration regime, $\lambda \leq 0.5$, relative to the ions.

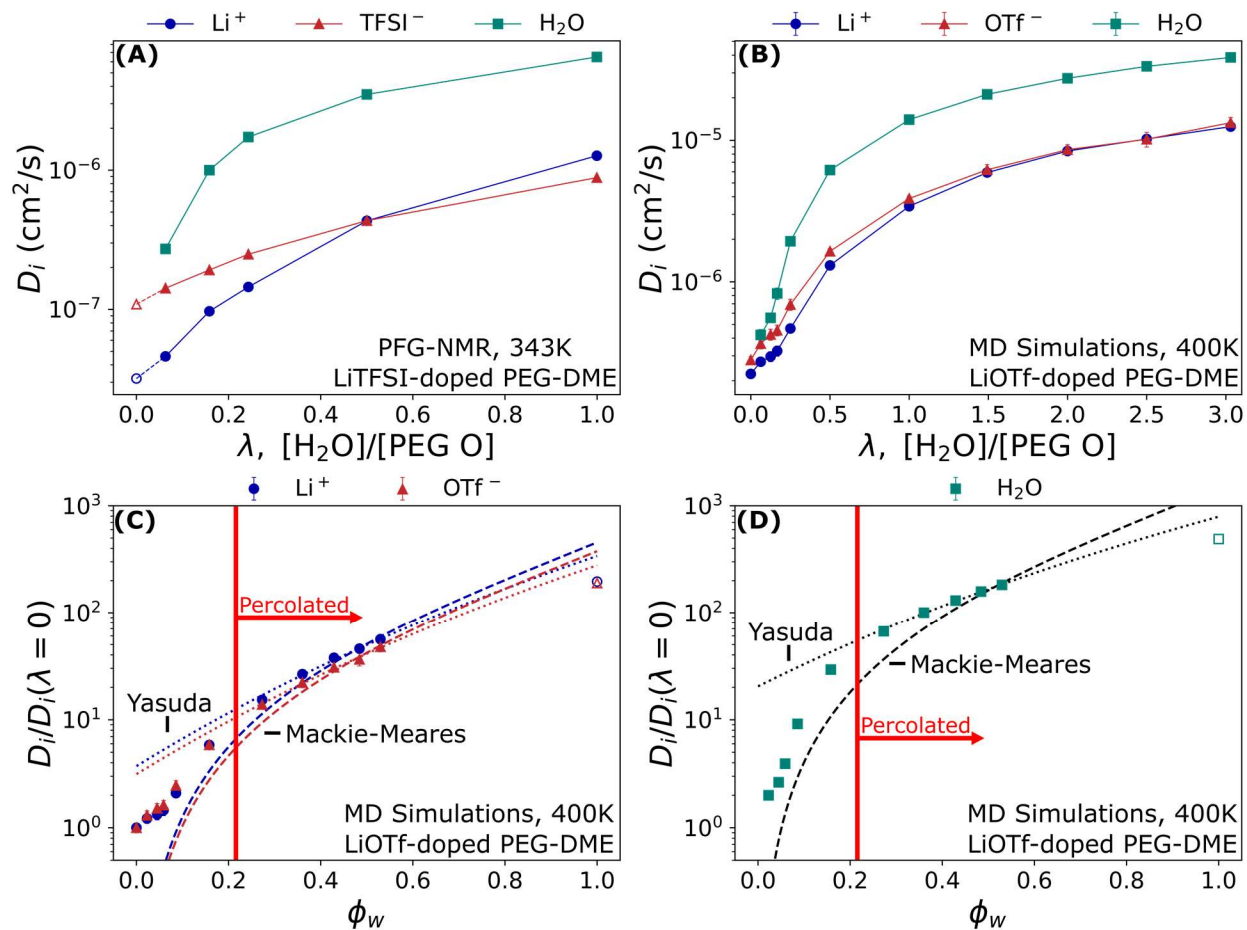


Figure 1: Ion and water diffusion coefficients as a function of hydration in (A) experimental LiTFSI-doped PEG-DME systems obtained using PFG-NMR, and (B) simulated LiOTf-doped PEG-DME systems. Experimental ion diffusivities under dry conditions ($\lambda = 0$, hollow points) were obtained from comparable experiments by Hayamizu et al.²⁸ Normalized (C) ion and (D) water diffusion coefficients (obtained from simulations) as a function of water volume fraction. Dashed and dotted lines represent the one-parameter Mackie-Meares (Equation 1) and two-parameter Yasuda (Equation 2) models fit to the diffusion coefficients at high hydration levels, respectively. Hollow points represent diffusion coefficients obtained from simulations of a 0.5 M aqueous salt solution at 400 K.

The experimental results presented in Figure 1A motivate the four questions examined in this study: 1) To what degree can the models used for hydrated polymer membranes (Equations 1 and 2) describe ion and water transport at low water content? 2) At low water content, does ion diffusion exhibit the same dependence on polymer segmental dynamics as in dry systems, and what is the role of ion-polymer solvation in such regimes? 3) What are the mechanisms underlying the diffusive speedup of Li^+ relative to TFSI^- ions? 4) What factors govern the speedup of water molecules relative to ions at low hydration levels?

Atomistic molecular dynamics (MD) simulations offer an opportunity to probe the mechanisms underlying the experimentally observed trends.^{13,27,29–32} In our study, atomistic MD simulations were initially performed on LiTFSI-doped PEG-DME (Figure S6, MW \approx 443 g/mol, 10 oxygen atoms per chain) across a wide range of hydration levels. However, our simulations exhibited water-polymer phase separation for $\lambda > 0.5$ for this specific force field (Figures S15A-17, see Section S3 for more information). Hence, we chose to focus instead on lithium trifluoromethanesulfonate (LiOTf)-doped PEG-DME, which could be simulated without phase separation (Figures S15B and S18) at the same salt loading as the experimental systems, $[\text{PEG O}]/[\text{LiOTf}] = 10$, across 11 water volume fractions, $\phi_w = 0.00$ to 0.53 ($\lambda = 0$ to 3 H_2O molecules per PEG oxygen atom, see Table S7) estimated assuming ideal volume additivity (Equation S10, see Figure S7). All simulations were performed at 400 K to simulate fast enough dynamics across the entire range of hydration levels and obtain sufficient statistics for self-diffusion measurements. While this is a higher temperature compared to experiments, the underlying physics is not expected to change significantly as a function of temperature, as seen in our simulations at dry conditions as a function of temperature (Figure 2A and B, see discussion

below). See Section S2.1-3 of the Supporting Information for more details on the simulation methodology, force field parameterization, and system setup, equilibration, and production.

Figure 1B displays the simulation results for ion (Li^+ , OTf^-) and water diffusivities as a function of λ . The evolution of the simulated diffusion coefficients with hydration level is qualitatively similar to that observed experimentally (Figure 1A). Specifically, we find that D_{Li^+} increases relative to D_{OTf^-} with increasing λ , although to a lesser degree than the increase in D_{Li^+} relative to D_{TFSI^-} observed experimentally. Further, a significant speedup in water dynamics is observed relative to ion dynamics at low hydration levels.

Figures 1C and D present the (C) ion (Li^+ , OTf^-) and (D) water diffusion coefficients (obtained from simulations) normalized by the diffusivity under dry conditions (ions: $D_i(\lambda = 0)$, water: $D_{\text{H}_2\text{O}}(\lambda \rightarrow 0)$) from a linear extrapolation of $\ln(D_{\text{H}_2\text{O}})$ vs. ϕ_w at low hydration levels²²) as a function of ϕ_w . The dashed and dotted lines represent the one-parameter (D_i^{Soln}) Mackie-Meares and two-parameter (D_i^{Soln}, β) Yasuda models, respectively. Section S2.5 contains more details on the fitting procedure. For reference, the normalized diffusion coefficients calculated for a 0.5 M aqueous salt solution at 400 K are plotted at $\phi_w = 1$ (See Section S2.3 for system details). Comparing the simulation results to predictions from the models, the diffusivities of water and ions at high ϕ_w are generally well described by both models. However, the low ϕ_w regime is poorly described, with the Mackie-Meares and Yasuda models under- and over-predicting the ion and water diffusivities, respectively.

Swollen polymer systems can be divided into two broad hydration regimes: low hydration regimes characterized by relatively small, non-percolating water clusters distributed throughout the polymer matrix, and higher hydration regimes characterized by a percolating tortuous water network with few to no isolated water clusters. To identify the transition between these regimes

for our system, in Figure S12A we plot the probability, $P(n)$, that a water molecule is associated with a water cluster of size n as a function of hydration. With increasing hydration, we observe a shift from a majority of one- or two-molecule clusters ($\lambda = 0.0625$ to 0.25) to moderately sized clusters with 10s to 100s of molecules ($\lambda = 0.5$) to a single large cluster (network) consisting of the majority of water molecules within the system ($\lambda = 1$ to 3). Figure S12B displays the fraction of water molecules associated with a percolated water network, defined as a water cluster with continuous association spanning both of its periodic images across one or more axes, as a function of hydration. Based on this analysis, we observe a clear transition from non-percolated to percolated water networks occurring around $\lambda = 0.5$ to 1.0 ($\phi_w = 0.158 - 0.273$). We combine the results of the above analysis with our diffusivity fits and add a red line separating the (left) non-percolated and (right) percolated water regimes in Figure 1C and D. Overall, we conclude that ion and water diffusion are well described by the existing models of hydrated membranes for regimes far above the percolation threshold.

To compare our diffusivity results for low hydration with the behavior in dry systems, we also performed MD simulations of dry LiOTf-doped PEG-DME at constant salt loading, $[\text{PEG O}]/[\text{LiOTf}] = 10$, as a function of temperature, $T = 400 - 500$ K. The characteristic relaxation times for both the hydrated and dry systems were calculated through the dynamical structure factor ($S(q, t)$) relaxation timescale at $q = 1.6 \text{ \AA}^{-1}$, τ_q (See Section S2.7 for more information). Figure 2A presents the ion diffusion coefficients as a function of inverse polymer segmental relaxation timescales normalized by the values at $\lambda = 0, T = 400$ K. Hollow and solid circles represent dry systems as a function of temperature and wet systems as a function of hydration, respectively. We observe a power law relationship between D and τ_q for both ions in dry systems as a function of temperature, denoted by the dashed line:

$$\frac{D_i(T)}{D_i(T = 400 \text{ K})} = \left(\frac{\tau_q(T = 400 \text{ K})}{\tau_q(T)} \right)^\gamma. \quad (3)$$

By comparison, hydrated systems exhibit significantly faster dynamics (as a function of τ_q for the hydrated systems) than dry systems.

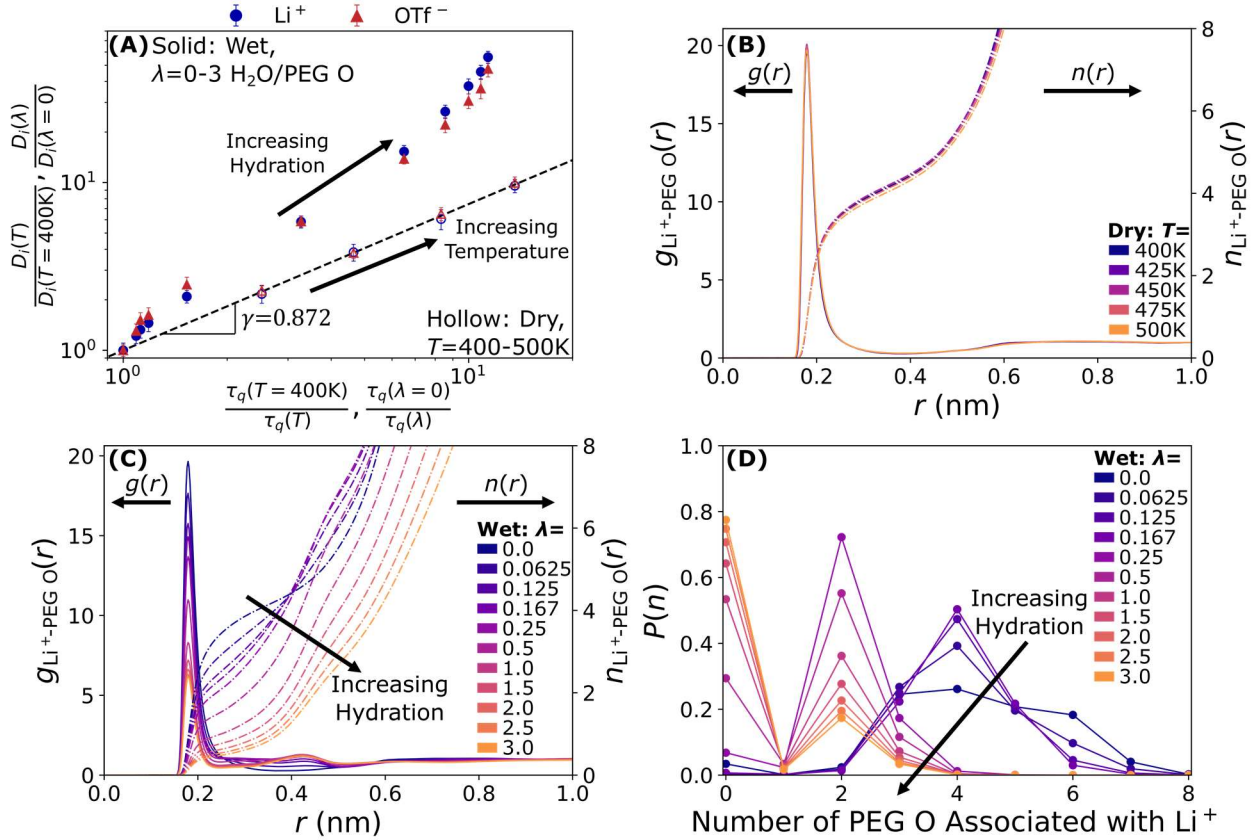


Figure 2: (A) Normalized ion diffusion coefficients as a function of normalized inverse polymer segmental relaxation timescales. Hollow and solid circles represent dry systems as a function of temperature and wet systems as a function of hydration, respectively. The dashed line represents the power-law fit to dry systems, $D \propto \tau_q^{-\gamma}$. Radial ($g(r)$, solid lines, left axis) and coordination ($n(r)$, dashed lines, right axis) distribution functions for Li⁺ – PEG O in (B) dry systems as a function of temperature and (C) wet systems as a function of hydration. (D) Probability that a Li⁺ ion is associated with n PEG O atoms as a function of hydration.

To understand the origin of the deviation of the relationship between D_i and τ_q in hydrated versus dry systems, we turn to Li^+ – PEG interactions, quantified by the radial distribution functions, $g_{ij}(r)$, and corresponding coordination distribution function, $n_{ij}(r)$, between atoms of species i and j (See Section S2.6 for more information). Figures 2B and C present the Li^+ – PEG O $g(r)$ and $n(r)$ for (B) dry systems as a function of temperature and (C) wet systems as a function of hydration. For dry systems, from Figure 2B we observe strong interactions ($g(r \sim 0.2 \text{ nm}) \gg 1$) between Li^+ ions and PEG O atoms and a significant coordination number of $n(r^* \sim 0.4 \text{ nm}) \approx 4.5$ PEG O atoms per Li^+ ion. Further, the solvation characteristics do not change as a function of temperature, rationalizing the strong correlation between temperature-induced diffusive speedup and τ_q . In contrast, for wet systems, we observe a significant reduction in the Li^+ – PEG O interaction strength (magnitude of the first peak, $g(r \sim 0.2 \text{ nm})$, decreases) with increasing hydration, and a corresponding decrease in the coordination number from $n(r^* \sim 0.4 \text{ nm}) \approx 4.5$ to $n(r^* \sim 0.3 \text{ nm}) \approx 0.5$ PEG O atoms per Li^+ ion (c.f. Figure 2C). Such results are observed more explicitly in Figure 2D, which presents the probability, $P(n)$, that a Li^+ ion is associated with n PEG O atoms as a function of hydration. From Figure 2D, we observe a shift from a broad distribution of Li^+ ions associating with 3-6 PEG O atoms under dry conditions, to a peak at $n = 4$ for low hydrations ($\lambda = 0.0625 - 0.167$), a majority peak at $n = 2$ for moderate hydrations ($\lambda = 0.25 - 0.5$), and a majority peak at $n = 0$ for the percolated regime ($\lambda \geq 1$).

Figure 3A presents the corresponding average number of water molecules associated to a Li^+ ion, n_w , normalized by the value in aqueous solution, n_w^{Soln} , as a function of hydration (see Section S2.6 for more details). As Li^+ disassociates from PEG with increasing hydration, it associates with water molecules. Specifically, we observe that an average Li^+ ion associates with

20 – 40% of its desired water coordination shell at low hydrations ($\lambda = 0.0625 - 0.167$), 50 – 60% at moderate hydrations ($\lambda = 0.25 - 0.5$), and 80 – 90% in the percolated regime ($\lambda \geq 1$). Based on the above results, in hydrated systems, the Li^+ ions are simultaneously solvated by the PEG O atoms and water molecules, with the degree of respective solvation influenced by membrane hydration. Hence, the motion of Li^+ ions is less coupled to the polymer segmental dynamics as the level of hydration increases, which explains the weaker correlation between D_{Li^+} and τ_q in hydrated systems compared to dry systems.

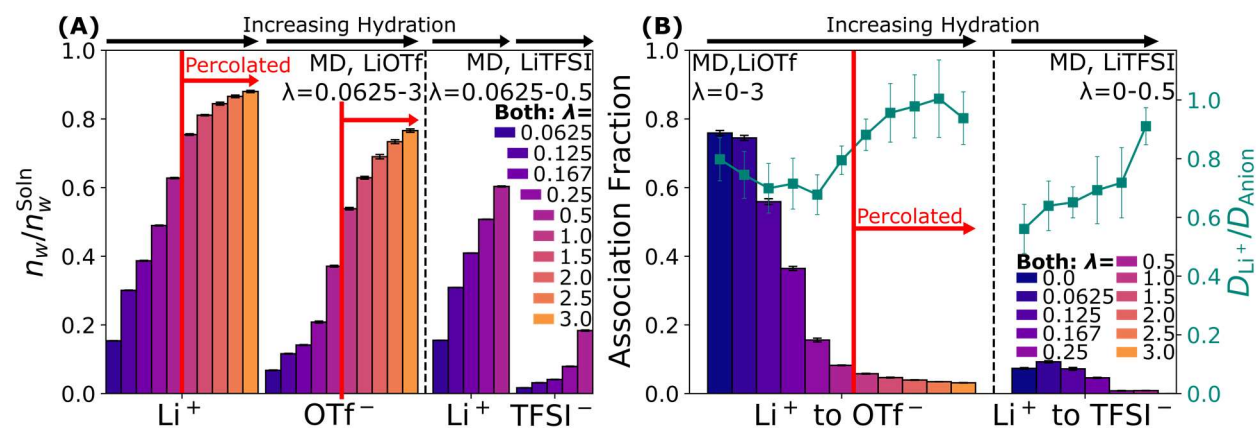


Figure 3: (A) Ratio of the number of water molecules in the first coordination shell of ions in membrane to that in an aqueous salt solution as a function of hydration. (B) Fraction of Li^+ ions associated with at least one anion (bars, left axis) and ratio of the Li^+ to anion diffusion coefficient (points, right axis) as a function of hydration. The vertical dashed lines separate results for (left) LiOTf-doped PEG-DME and (right) LiTFSI-doped PEG-DME. All results were obtained from MD simulations.

Now, we turn to the mechanisms underlying the diffusivity of the anions. We hypothesize that anion diffusion is influenced by anion-water solvation and Li^+ -anion electrostatic interactions. From the ion solvation characteristics presented in Figure 3A for LiOTf, Li^+ exhibits a more complete hydration shell than OTf^- , especially in the non-percolated regime. Thus, Li^+ should

exhibit a stronger hydration-induced diffusive speedup than OTf^- . However, in the non-percolated regime, from Figure 3B, which presents the fraction of Li^+ ions associated with at least one anion (bars, left axis), we observe a significant degree of ion pairing (i.e., cation-anion association, see Section S2.6) between Li^+ and OTf^- ions. Such strong attractive electrostatic interactions are expected to couple the ion dynamics, such that the speedup of a partially hydrated Li^+ ion induces a similar speedup in the diffusion of a paired OTf^- ion. Together, such factors rationalize the hydration-induced speedup of OTf^- ions. However, Li^+ ions exhibit a slightly more pronounced speedup compared to OTf^- ions (Figure 1B) due to the more complete hydration shell exhibited by Li^+ relative to OTf^- ions.

We recall that the experimental system of LiTFSI exhibited a more pronounced speedup of Li^+ relative to TFSI^- ions (Figure 1A) compared to our simulations for LiOTf (also seen in simulations of LiTFSI-doped PEG-DME at low hydrations, Figure 3B – see Section S3 for more information). The above reasoning also explains such observations. Indeed, in LiTFSI systems, TFSI^- exhibits significantly weaker solvation by water relative to Li^+ (Figure 3A) as a function of hydration compared to OTf^- and Li^+ . Further, the bulkier TFSI^- exhibits much less cation-anion pairing relative to OTf^- (Figure 3B), reducing the influence of Li^+ dynamics on the anions. As a result, while both Li^+ and TFSI^- ions exhibit a hydration-induced increase in diffusivity, there is a much more pronounced speedup of the Li^+ relative to TFSI^- ions (Figure 3B).

Finally, we hypothesize the diffusivity trends of water noted in Figures 1A and B to arise from the interplay between $\text{Li}^+ - \text{H}_2\text{O}$ solvation interactions and the formation of water clusters. To support this, in Figure 4A we present the fraction of water molecules associated with Li^+ ions as a function of hydration in LiOTf-doped systems. The fraction of water molecules solvating Li^+ ions decreases from encompassing nearly all water molecules at very low hydrations to less than

half of the water molecules in the percolated regime. At low water content, Li^+ -solvating water molecules are dynamically bound over a long timescale (Figure S11, see Section S2.6 for more information), and therefore are expected to exhibit highly coupled dynamics with the relatively slower Li^+ ions. With increasing hydration, the rise in non-solvating water molecules as clusters/networks (Figure S12A) is expected to facilitate independent and faster water dynamics.

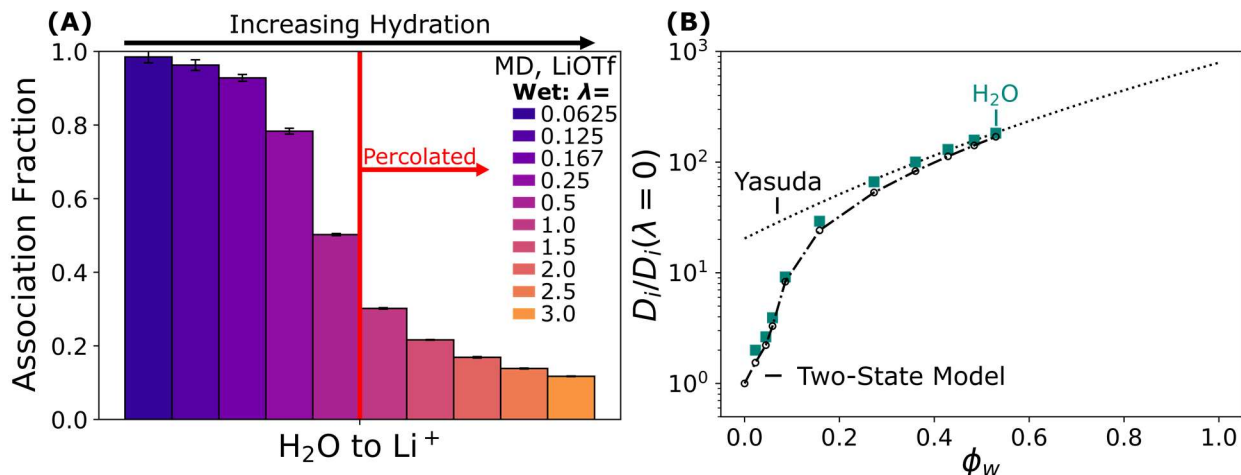


Figure 4: (A) Fraction of water molecules associated with Li^+ ions as a function of hydration. (B) Normalized water diffusion coefficients as a function of water volume fraction calculated from MD simulations. The dotted line represents the Yasuda free volume model ($D_{\text{H}_2\text{O}}^{\text{Yasuda}}$) fit to water diffusivities at high hydration (See Section S2.5). The dash-dot line represents the two-state model for predicting water diffusivities based on $\text{H}_2\text{O} - \text{Li}^+$ association fractions, D_{Li^+} , and $D_{\text{H}_2\text{O}}^{\text{Yasuda}}$.

To validate our picture of water transport, we describe water diffusion using a two-state model whereby lithium-solvating water molecules diffuse with their Li^+ ions (D_{Li^+}), and unassociated water molecules diffuse within water clusters whose diffusivity can be described by the Yasuda model ($D_{\text{H}_2\text{O}}^{\text{Yasuda}}$):

$$D_{\text{H}_2\text{O}}^{\text{Two-State}} = x_{\text{solv}} D_{\text{Li}^+} + (1 - x_{\text{solv}}) D_{\text{H}_2\text{O}}^{\text{Yasuda}}, \quad (4)$$

where x_{solv} is the fraction of water molecules associated with Li^+ ions. Figure 4B displays the normalized water diffusion coefficients (points), Yasuda model fit (See Section S2.5) as presented in Figure 1D (dotted line), and the two-state model (dash-dot line) as a function of ϕ_w . We note that D_{Li^+} and x_{solv} are values calculated from the MD simulations as presented in Figures 1B, C and Figure 4A, respectively. We observe very good agreement between the two-state model prediction and diffusion coefficients calculated from MD simulations, which supports our molecular description of water transport.

In summary, we have combined PFG-NMR diffusivity measurements and atomistic MD simulations to probe ion and water transport in salt-doped PEG-DME in the transition from dry to swollen hydrogel networks. The transport characteristics can be broadly divided into two distinct regimes, non-percolated and percolated water networks. The percolated regime is shown to be well-described by the relatively simple Mackie-Meares hindered transport and Yasuda free volume models. To probe the diffusion mechanism in the non-percolated regime, we first compared weakly hydrated systems to dry systems as a function of temperature, within which ion-polymer solvation is critical and ion transport is well known to be strongly correlated with polymer segmental dynamics. We observed a significant deviation from this correlation with the addition of water, which we attributed to the weakening of $\text{Li}^+ - \text{PEG}$ solvation in favor of $\text{Li}^+ - \text{H}_2\text{O}$ solvation, which leads to faster Li^+ dynamics. Anion dynamics can be described by the interplay between cation-anion and anion-water interactions. Lastly, water dynamics can be described by a simple two-state model, embodying a combination of $\text{Li}^+ - \text{H}_2\text{O}$ coupled dynamics and free volume diffusion of non-solvating waters. Our findings provide a more encompassing analysis of ion and water transport in hydrated polymer electrolytes, specifically in the low hydration, non-percolated regime.

Acknowledgements

This work was supported as part of the Center for Materials for Water and Energy Systems (M-WET), an Energy Frontier Research Center funded by the U.S. Department of Energy, Office of Science, Basic Energy Sciences, under Award #DE-SC0019272. The NMR measurements made use of shared facilities of the National Science Foundation (NSF)-supported Materials Research Science and Engineering Center (MRSEC) at UC Santa Barbara, NSF DMR-2308708. The UCSB MRSEC is a member of the Materials Research Facilities Networks (www.mrfn.org). V.G. acknowledges support from the Robert A. Welch Foundation (F-1599) to support the salary of Z.Z. The results in this paper were generated using high-performance computing resources provided by The University of Texas at Austin Texas Advanced Computing Center.

Supporting Information Available

Section S1, details of the experimental materials, methodology, and supplementary results; Section S2 details of the computational system methodology, force field parameters, methodology, and supplementary results; Section S3 details of supplementary results for LiTFSI-doped PEG-DME simulations.

References

- (1) Long, L.; Wang, S.; Xiao, M.; Meng, Y. Polymer Electrolytes for Lithium Polymer Batteries. *J. Mater. Chem. A* **2016**, *4* (26), 10038–10069.
- (2) Arya, A.; Sharma, A. L. Polymer Electrolytes for Lithium Ion Batteries: A Critical Study. *Ionics (Kiel)* **2017**, *23* (3), 497–540.
- (3) Hallinan Jr, D. T.; Balsara, N. P. Polymer Electrolytes. *Annu. Rev. Mater. Sci.* **2013**, *43*, 503–525.

- (4) Zhou, D.; Shanmukaraj, D.; Tkacheva, A.; Armand, M.; Wang, G. Polymer Electrolytes for Lithium-Based Batteries: Advances and Prospects. *Chem* **2019**, *5* (9), 2326–2352.
- (5) Shin, D. W.; Guiver, M. D.; Lee, Y. M. Hydrocarbon-Based Polymer Electrolyte Membranes: Importance of Morphology on Ion Transport and Membrane Stability. *Chem. Rev.* **2017**, *117* (6), 4759–4805.
- (6) Geise, G. M.; Paul, D. R.; Freeman, B. D. Fundamental Water and Salt Transport Properties of Polymeric Materials. *Prog. Polym. Sci.* **2014**, *39* (1), 1–42.
- (7) Luo, T.; Abdu, S.; Wessling, M. Selectivity of Ion Exchange Membranes: A Review. *J. Membr. Sci.* **2018**, *555*, 429–454.
- (8) Geise, G. M.; Lee, H.-S.; Miller, D. J.; Freeman, B. D.; McGrath, J. E.; Paul, D. R. Water Purification by Membranes: The Role of Polymer Science. *J. Polym. Sci. B Polym. Phys.* **2010**, *48* (15), 1685–1718.
- (9) Nandi, A.; Rakshit, A.; Banerjee, P. Resource Recovery from Wastewater Using Polymeric Membranes. In *Membranes for Water Treatment and Remediation*; Springer, 2023; pp 227–248.
- (10) Sujanani, R.; Landsman, M. R.; Jiao, S.; Moon, J. D.; Shell, M. S.; Lawler, D. F.; Katz, L. E.; Freeman, B. D. Designing Solute-Tailored Selectivity in Membranes: Perspectives for Water Reuse and Resource Recovery. *ACS Macro Lett.* **2020**, *9* (11), 1709–1717.
- (11) Druger, S. D.; Nitzan, A.; Ratner, M. A. Dynamic Bond Percolation Theory: A Microscopic Model for Diffusion in Dynamically Disordered Systems. I. Definition and One-Dimensional Case. *J. Chem. Phys.* **1983**, *79* (6), 3133–3142.

- (12) Nitzan, A.; Ratner, M. A. Conduction in Polymers: Dynamic Disorder Transport. *J. Phys. Chem.* **1994**, *98* (7), 1765–1775.
- (13) Borodin, O.; Smith, G. D. Mechanism of Ion Transport in Amorphous Poly (Ethylene Oxide)/LiTFSI from Molecular Dynamics Simulations. *Macromolecules* **2006**, *39* (4), 1620–1629.
- (14) Maitra, A.; Heuer, A. Cation Transport in Polymer Electrolytes: A Microscopic Approach. *Phys. Rev. Lett.* **2007**, *98* (22), 227802.
- (15) Diddens, D.; Heuer, A.; Borodin, O. Understanding the Lithium Transport within a Rouse-Based Model for a PEO/LiTFSI Polymer Electrolyte. *Macromolecules* **2010**, *43* (4), 2028–2036.
- (16) Pesko, D. M.; Webb, M. A.; Jung, Y.; Zheng, Q.; Miller III, T. F.; Coates, G. W.; Balsara, N. P. Universal Relationship between Conductivity and Solvation-Site Connectivity in Ether-Based Polymer Electrolytes. *Macromolecules* **2016**, *49* (14), 5244–5255.
- (17) Zhang, H.; Geise, G. M. Modeling the Water Permeability and Water/Salt Selectivity Tradeoff in Polymer Membranes. *J. Membr. Sci.* **2016**, *520*, 790–800.
- (18) Jang, E.-S.; Kamcev, J.; Kobayashi, K.; Yan, N.; Sujanani, R.; Dilenschneider, T. J.; Park, H. B.; Paul, D. R.; Freeman, B. D. Influence of Water Content on Alkali Metal Chloride Transport in Cross-Linked Poly (Ethylene Glycol) Diacrylate. 2. Ion Diffusion. *Polymer (Guildf)* **2020**, *192*, 122316.
- (19) Yan, N.; Sujanani, R.; Kamcev, J.; Jang, E.-S.; Kobayashi, K.; Paul, D. R.; Freeman, B. D. Salt and Ion Transport in a Series of Crosslinked AMPS/PEGDA Hydrogel Membranes. *J. Membr. Sci.* **2022**, *653*, 120549.

- (20) Mackie, J. S.; Meares, P. The Diffusion of Electrolytes in a Cation-Exchange Resin Membrane I. Theoretical. *Proc. R. Soc. Lond. A: Math. Phys. Eng. Sci.* **1955**, *232* (1191), 498–509.
- (21) Cohen, M. H.; Turnbull, D. Molecular Transport in Liquids and Glasses. *J. Chem. Phys.* **1959**, *31* (5), 1164–1169.
- (22) Yasuda, H.; Lamaze, C. E.; Peterlin, A. Diffusive and Hydraulic Permeabilities of Water in Water-Swollen Polymer Membranes. *J. Polym. Sci. A2* **1971**, *9* (6), 1117–1131.
- (23) Ludwig, K. B.; Correll-Brown, R.; Freidlin, M.; Garaga, M. N.; Bhattacharyya, S.; Gonzales, P. M.; Cresce, A. V; Greenbaum, S.; Wang, C.; Kofinas, P. Examining the Electrochemical Properties of Hybrid Aqueous/Ionic Liquid Solid Polymer Electrolytes through the Lens of Composition-Function Relationships. *Adv. Energy Mater.* **2023**, *13* (31), 2301428.
- (24) Ludwig, K. B.; Correll-Brown, R.; Freidlin, M.; Garaga, M. N.; Bhattacharyya, S.; Gonzales, P. M.; Cresce, A. V; Greenbaum, S.; Wang, C.; Kofinas, P. Highly Conductive Polyacrylonitrile-Based Hybrid Aqueous/Ionic Liquid Solid Polymer Electrolytes with Tunable Passivation for Li-Ion Batteries. *Electrochim. Acta* **2023**, *453*, 142349.
- (25) Park, J. H.; Jung, S.; Handayani, P. L.; Aluru, N.; Kim, T.; Lee, S. B.; Choi, U. H.; Lee, J. Enthalpic and Entropic Contributions to Fast Lithium Ion Conduction in Solid-State Aqueous Polymer Electrolytes. *J. Phys. Chem. C* **2022**, *126* (39), 16777–16784.
- (26) Zhang, J.; Cui, C.; Wang, P.-F.; Li, Q.; Chen, L.; Han, F.; Jin, T.; Liu, S.; Choudhary, H.; Raghavan, S. R.; Eidson, N.; von Cresce, A.; Ma, L.; Uddin, J.; Addison, D.; Yang, C.;

- Wang Chunsheng. “Water-in-Salt” Polymer Electrolyte for Li-Ion Batteries. *Energy Environ. Sci.* **2020**, *13* (9), 2878–2887.
- (27) Widstrom, M. D.; Borodin, O.; Ludwig, K. B.; Matthews, J. E.; Bhattacharyya, S.; Garaga, M.; V. Cresce, A.; Jarry, A.; Erdi, M.; Wang, C.; Greenbaum, S.; Kofinas, P. Water Domain Enabled Transport in Polymer Electrolytes for Lithium-Ion Batteries. *Macromolecules* **2021**, *54* (6), 2882–2891.
- (28) Hayamizu, K.; Akiba, E.; Bando, T.; Aihara, Y. ^1H , ^7Li , and ^{19}F Nuclear Magnetic Resonance and Ionic Conductivity Studies for Liquid Electrolytes Composed of Glymes and Polyetheneglycol Dimethyl Ethers of $\text{CH}_3\text{O}(\text{CH}_2\text{CH}_2\text{O})_n\text{CH}_3$ ($N= 3\text{--}50$) Doped with $\text{LiN}(\text{SO}_2\text{CF}_3)_2$. *J. Chem. Phys.* **2002**, *117* (12), 5929–5939.
- (29) Wheatle, B. K.; Keith, J. R.; Mogurampelly, S.; Lynd, N. A.; Ganesan, V. Influence of Dielectric Constant on Ionic Transport in Polyether-Based Electrolytes. *ACS Macro Lett.* **2017**, *6* (12), 1362–1367.
- (30) Molinari, N.; Mailoa, J. P.; Kozinsky, B. Effect of Salt Concentration on Ion Clustering and Transport in Polymer Solid Electrolytes: A Molecular Dynamics Study of PEO-LiTFSI. *Chem. Mater.* **2018**, *30* (18), 6298–6306.
- (31) Zofchak, E. S.; Zhang, Z.; Marioni, N.; Sachar, H. S.; Freeman, B. D.; Ganesan, V. Cation–Polymer Interactions and Local Heterogeneity Determine the Relative Order of Alkali Cation Diffusion Coefficients in PEGDA Hydrogels. *J. Membr. Sci.* **2023**, *685*, 121898.
- (32) Nordness, O.; Moon, J. D.; Marioni, N.; Zofchak, E. S.; Richardson, P. M.; Landsman, M. R.; Katz, L. E.; Hawker, C. J.; Ganesan, V.; Segalman, R. A.; Clément, R. J. Probing

Water and Ion Diffusion in Functional Hydrogel Membranes by PFG-NMR.

Macromolecules **2023**, *56* (12), 4669–4680.

For Table of Contents Only

